TECHNICAL MEMORANDUMS

NATIONAL ADVISORY COMMITTEE FOR AERONAUTICS

No. 986

NEW FRICTIONAL RESISTANCE LAW FOR SMOOTH PLATES

By F. Schultz-Grunow

NATIONAL ADVISORY COMMITTEE FOR AERONAUTICS

TECHNICAL MEMORANDUM NO. 986

NEW FRICTIONAL RESISTANCE LAW FOR SMOOTH PLATES*

By F. Schultz-Grunow

SUMMARY

From measurements in the free boundary layer of a
plate the laws governing the velocity distribution and a
new resistance law are derived which, by increasing
Reynolds number Re_x afford lower resistance values than
the logarithmic law. The transverse velocities, the shear-
ing stress, and the mixing path profiles were also defined.

INTRODUCTION

The application of the logarithmic laws of velocity
distribution for turbulent pipe flow (reference 1) to the
free friction layer had afforded a resistance law which,
after minor changes of the experimental constants contained
in the velocity distribution laws, could be brought into
satisfactory agreement with the plate drag measurements, up
to the highest Re_x numbers.

Nevertheless, this application constitutes no more
than an approximation for the still unknown velocity dis-
tribution in the free friction layer, for there is no cogent
necessity for an identical velocity distribution in the
pipe and on the plate; one may only surmise that they dif-
fer slightly from one another. Aside from that the plate
drag measurements (references 2 and 3) are not completely
satisfactory, since they were achieved with comparatively
small test plates on which the assumption of plane flow is
not only in the neighborhood of the plate leading edge or
else obtained on not completely hydraulically smooth plates
(reference 4). It therefore seemed desirable to explore
the velocity distribution in the free friction layer and
to check the drag measurements.

Notation

x distance from plate leading edge – coordinate of plate length

y wall distance

z coordinate of plate width

l mixing path

u velocity in direction x

$\bar{u}$ mean velocity in friction layer

U flow velocity

v velocity in direction y

τ shearing stress

τ_0 wall shearing stress

ρ density

$v^* = \sqrt{\dfrac{\tau_0}{\rho}}$ rate of shearing stress

δ friction layer thickness

$\delta^* = \displaystyle\int_0^\delta \left(1 - \frac{u}{U}\right) dy$ displacement thickness

$\vartheta = \displaystyle\int_0^\delta \frac{u}{U}\left(1 - \frac{u}{U}\right) dy$ momentum thickness

$c_f' = \dfrac{\tau_0}{\frac{\rho}{2} U^2}$ local drag coefficient

$c_f = \dfrac{\displaystyle\int_0^x \tau_0\, dx}{\frac{\rho}{2} U^2 x}$ total drag coefficient

v kinematic viscosity

$$Re_x = \frac{U\ x}{v}$$

$$Re_\delta = \frac{\overline{u}\ \delta}{v}$$
$\left.\vphantom{\begin{array}{c}a\\b\\c\end{array}}\right\}$ Reynolds numbers

EXPERIMENTAL SET-UP

The measurements were to be made in the tunnel so as to insure greater accuracy, while at the same time the conditions on free surfaces were to be preserved; i.e., no pressure decrease, and a free friction layer, which means that the friction layer is followed by a parallel flow with constant velocity distribution. A newly erected experimental arrangement for air operation was employed. It consisted essentially of a blower-operated tunnel of rectangular section (fig. 1), the lower, horizontally placed wall of which carried the surface to be explored. The aspect ratio of the cross section was chosen with a view to plane flow in the median zone of the horizontal sides. The tunnel height was so chosen that the opposite friction layers were always kept separate by the nuclear flow, that is, the zone of uniformly distributed speed U in figure 1, and thus produced free friction layers. The upper wall of the tunnel was hinged and adjustable so that any prescribed pressure distribution and, for our purposes, also a pressure equal to the outside pressure could be obtained to within 1/20 millimeter alcohol accuracy. The tunnel height thereby increased in flow direction according to the proportional growth of the displacement thickness at the walls. This made the conditions in the tunnel the same as on free surfaces.

That the flow in the median zone of the test plate is in fact plane can be seen on the velocity profiles in figure 2 plotted against the logarithm of the wall resistance y, as recorded in a plane at right angles to flow direction and experimental wall, in the tunnel center (z = 0) and 250 millimeters to the left (z = -250) and right (z = 250) of it as viewed in flow direction. The intermediate profiles, which were also recorded and lie in the same range of scattering, have been omitted for reasons of clarity.

To make sure that the transitional region was definitely situated on the plate leading edge, this edge was greatly curved, and, to insure the formation of a new friction layer on it, a slot was provided below this edge through which the friction layer of the blower chamber wall exhausted (fig. 1).

RESISTANCE MEASUREMENT

There were two ways of measuring the frictional re-
sistance. The momentum loss $\dfrac{d}{dx}\displaystyle\int_0^{\delta} u(U-u)dy$ could be
determined from the measurement of the dynamic pressure
over wall distance y at different distances x from
the plate leading edge and the wall shearing stress τ_0,
then computed from the momentum equation.

$$\tau_0/\rho = \frac{d}{dx}\int_0^{\delta} u(U-u)dy \qquad (1)$$

Or the friction could be weighed directly on a rectangular
test plate mounted movably in a sector of the principal
plate. The latter method proved more accurate. A similar
method had already been used elsewhere (reference 3). The
arrangement is illustrated in figure 3. The test plate
rests on an arm in flexure pivots F rotatable about a
vertical axis. The weight is taken up by a float S.
Aside from the moment of the friction force an opposite
moment is applied in the hinge by a wire D stressed in
torsion. The wire can be twisted with the hand wheel un-
til it balances the moment of the friction force and the
scale arm is in the neutral setting, which can be read
optically. The torque for the related twist was calibrat-
ed so that the frictional force and hence the local resist-
ance could be ascertained. This arrangement is practical
only in our case, where the pressure in the tunnel is the
same as in the outside space. In any other case the slots
in the sector necessary for the free movement of the test
plate manifest flows which produce uneven suction and pres-
sure on the plate edges and falsify the measurement.

Three surfaces were explored. Surface A was a
built-up plywood plate of 25 millimeters thickness; surface
B, the puttied, polished, and lacquered surface of a high-
power metal airplane; and surface C consisted of separate,
1.5 millimeter thick metal panels arranged as in figure 4,
flush riveted on a 1.5 millimeter thick metal plate. The
whole was fastened with countersunk wood screws to a braced
plywood plate and, without prior puttying, given a smooth
camouflage coat.

Surface A.- The momentum, displacement, and friction-layer thickness obtained from the velocity measurements are reproduced in figure 5. The next question was whether the zero point of the diagram could be permitted to coincide with the plate leading edge, because the leading edge of the test plate was of finite thickness and was rounded off. Only a minor correction was disclosed by recalculation of the plate length from the friction-layer thickness obtained in the foremost test section $(x = 0.25$ m$)$ by the old power law (reference 5), which at small Reynolds numbers corresponds to reality quite well.

The momentum thickness ϑ can be tied to the drag coefficients through equation (1). It affords with the equation for ϑ:

$$c_f{}' = 2 \frac{d\vartheta}{dx} \tag{2a}$$

$$c_f = 2 \frac{\vartheta}{x} \tag{2b}$$

so that the drag coefficients can be determined from the measured momentum thickness. But this determination was found to be not accurate enough. The scale measurements shown in figure 6 are much more accurate. A curve I included for comparison reproduces the resistance law (reference 1) obtained with the logarithmic velocity distribution law for flow in pipes, curve II the old power law (reference 5) and curve III an empirical system of formulas (reference 6).

$$c_f = \frac{0.242}{\log(Re_x \, c_f)} \tag{3a}$$

$$c_f{}' = \frac{0.558 \, c_f}{0.558 + 2\sqrt{c_f}} \tag{3b}$$

obtained from all the plate measurements made up to that time.

It may be mentioned that (3a) and the so-called Schlichting approximate formula (reference 1)

$$c_f = \frac{0.455}{(\log Re_x)^{2.58}} \tag{4}$$

which refers to curve I are practically in accord within
our range of experimentation.

Figure 6 manifests a systematic departure of the
equalizing curve IV of our measurements from curve I to
the extent that the new measurements give lower drag
coefficients at log Re_x = 7.2 for instance, the values
are 4 percent lower. At any rate, surface A proved hy-
draulically smooth under the conditions of our measrue-
ments.

As to the accuracy of these measurements it should
be added that the test surface was slightly wavy, since a
technical surface was involved. Even though it did not
show up as roughness, the plate nevertheless manifested
areas where the edges of the test plate stood out or back
a little, thus inducing slot flows. But the effect of
these flows could be nullified by the design of the lead-
ing and trailing edges of the plate shown in figure 3. A
0.1-millimeter vertical displacement of the plate on the
scale produced a 1.5 percent change in force. Since the
plate height could be accurately adjusted to 0.1 milli-
meter, this percentage is the degree of the test accuracy.

On surfaces B and C the accuracy was substantially
less. First, because the test length was only 2 meters
instead of 6 meters; then, no suitable pressure orifices
could be provided on the surfaces without causing inter-
ference; hence zero pressure could not be reliably ob-
tained; and lastly, the edges of the plate could not,
without destroying their surface, be sharpened in the
requisite manner so as to minimize the effect of the slot
flow properly. Thus a 0.1-millimeter vertical displace-
ment of the test plate had already yielded a 6-percent
change in force, and so it may be stated merely that the
test values scattered around the power law and that the
surfaces are likewise hydraulically smooth within the ex-
plored range (to Re_x = 10^7).

VELOCITY DISTRIBUTION

The laws of velocity distribution in the free fric-
tion layer are derived from the same points of view as
for pipe flow (reference 1). There are two such laws
(reference 7), one for wall proximity, the other for the
remaining zone of the friction layer (reference 1). The

first resulted from the fact that in wall proximity the
wall distance is the characteristic quantity for the
flow attitude. It is expressed with

$$\frac{u}{v^*} = f_1 \left(\frac{v^* y}{\upsilon} \right) \qquad\qquad (5a)$$

For not too close wall proximity it is

$$\frac{u}{v^*} = A \log \frac{yv^*}{\upsilon} + B \qquad\qquad (5b)$$

where A and B are universal constants and defined from
the test. The second law stems from the argument that the
similitude of the flow at greater wall distances is solely
defined by the pipe radius and the friction layer thickness
δ, respectively. Here it affords

$$\frac{U - u}{v^*} = f_2 \left(\frac{y}{\delta} \right) \qquad\qquad (6)$$

On the pipe f_2 can be fairly approximated from (5b);
hence the wall proximity law may be extrapolated over the
pipe radius. The velocity measurements in figures 7 and
8, in fact, disclose that the test points in wall proximity
and in wall distance, respectively, form one curve. This
is particularly so in figure 8 across the entire test
range with exception of the test point closest to the wall.
In this plot the test points near the wall terminate in a
straight line, a sign that the linear wall law (5b) is
applicable, as is plainly seen in figure 7. The constants
here assume the values

$$A_P = 5.93, \qquad B_P = 4.07$$

subscript P denoting the plate. The pipe tests on the
other hand (reference 1) had given

$$A_R = 5.74, \qquad B_R = 5.46 *$$

---

*These values correspond to average values of smaller and
larger Reynolds numbers used as a basis for the determina-
tion of the logarithmic resistance law. For large Reynolds
numbers the values $A_R = 5.84$ and $B_R = 5.52$ are better.

In the calculation of the logarithmic law of plate
resistance (reference 1) with equation (5b) these constants
were modified to

$$A_R' = 5.85, \quad B_R' = 5.56$$

so as to afford agreement with Kempf's experiments (refer-
ence 3). Therefore, discounting the minor discrepancy
in the experimental constants the same wall proximity law
as in the pipe is applicable. However, figure 8 shows in
the wall distance even more than in pipe flow a distinct
departure from this law, to the extent that the test points
deflect downward from the straight line in order to reach
the abscissa before the straight line. In this instance
the application of the pipe flow to the plate affords
therefore a less good approximation, for the straight line

gives $\dfrac{U - u}{v^*} = 0$ at a too large abscissa value and, since

the friction layer thickness is defined with this value,
this thickness was computed a little too high, the momen-
tum loss too great and hence a drag a little too high.
This explains the discrepancy of our drag measurements
from the logarithmic resistance law.

Figure 8 shows, as has been mentioned, a universal
relationship with y/δ nearly throughout the entire test
range. Only the test point nearest the wall diverges and
thereby manifests the viscosity effect in the immediate
proximity of the wall. The range of the y/δ relation
in the individual test series fluctuates between $0.0039 \leq$
$\dfrac{y_1}{\delta} \leq 0.02$, to which values $\log \dfrac{y_1 v^*}{v} = 1.2$ corresponds

to subscript 1 denoting the limit of validity. In the
presence of the smallness of y_1/δ it is questionable
whether it is permissible to continue the straight line
in figure 8 as far as the wall. The question gains in
importance in the subsequent determination of the resist-
ance law, because of the required integration over y.
It is therefore checked on the integrals

$$\int_0^1 f_2 d\left(\frac{y}{\delta}\right), \quad \int_0^1 f_2^2 d\left(\frac{y}{\delta}\right).$$ With the curve in figure 8

it affords

$$\int_0^1 f_2 d\left(\frac{y}{\delta}\right) = 3.34; \quad \int_0^1 f_2^2 d\left(\frac{y}{\delta}\right) = 21.4$$

To check these values against the test, by transforming with (6) to

$$\int_0^1 f_2\left(\frac{y}{\delta}\right) d\left(\frac{y}{\delta}\right) = \frac{U}{v^*}\frac{\delta^*}{\delta} \qquad (7a)$$

$$\int_0^1 f_2{}^2\left(\frac{y}{\delta}\right) d\left(\frac{y}{\delta}\right) = \left(\frac{U}{v^*}\right)^2 \frac{\delta^* - \vartheta}{\delta} \qquad (7b)$$

$\frac{U}{v^*}$ was determined with the compensating curve IV of figure 6, according to the relation $\left(\frac{v^*}{U}\right)^2 = 2c_f{}'$. The integrals subsequently obtained in figure 5 are given in the table. They vary very little from the constant mean values which are in complete agreement with the previously secured values, so that the extrapolation as far as the wall is definitely permissible. With these data the relations for the displacement and momentum thickness follows from (7) at

$$\frac{\delta^*}{\delta} = 2.36 \sqrt{c_f{}'} ; \qquad \frac{\vartheta}{\delta} = \frac{\delta^*}{\delta} - 10.7\ c_f{}'$$

RESISTANCE LAW

At first it might be thought expedient without regard to the established velocity distribution to retain the logarithmic resistance law and to bring it into accord with the compensating cuve IV of figure 6 by subsequent change of the constants A_R, B_R. But that is not possible, as it merely would afford a parallel shift of the old curve I; whereas curve IV has a distinctly different inclination and hence would require a rotation of curve I also.

The new plate resistance law is therefore derived from equation (1) on the basis of our universal velocity distribution (fig. 8). The function f_2 may be introduced in (1), since its extrapolation as far as the wall has proved permissible. It affords with (7)

$$\left(\frac{v^*}{U}\right)^2 = \frac{d}{dx}\left[\delta\left(\frac{v^*}{U}\int_0^1 f_2 d\frac{y}{\delta} - \left(\frac{v^*}{U}\right)^2 \int_0^1 f_2{}^2 d\frac{y}{\delta}\right)\right]$$

and, with the above values for the integrals, after replacing x, $\delta : Re_x$, Re_δ :

$$\left(\frac{v^*}{U}\right)^2 = \frac{d}{d\,Re_x}\left[Re_\delta\left(3.34\,\frac{v^*}{U} - 21.4\left(\frac{v^*}{U}\right)^2\right)\right] \qquad (8)$$

As for the two unknown functions $\frac{v^*}{U}$, Re_δ for which a relation is necessary, it may be stated that the velocity distribution can be tied in with y/δ as well as $\frac{yv^*}{\nu}$, as previously indicated on equations (5) and (6). Specifically the relation

$$\frac{u}{v^*} = a_1 + b\,\ln\frac{yv^*}{\nu} \qquad (9a)$$

$$\frac{U-u}{v^*} = a_2 - b\,\ln\frac{y}{\delta} \qquad (9b)$$

affords from its identity the desired relation

$$\frac{U}{v^*} = a_1 + a_2 + b\,\log\frac{v^*\delta}{\nu}$$

or

$$Re_\delta = \frac{U}{v^*}\,e^{\frac{1}{b}\left(\frac{U}{v^*} - a\right)} \qquad (10)$$

with $a = a_1 + a_2$.

Now the tangent of the velocity distribution in a point of the wall adjacent viscid fluid layer is to be expressed by (9), a and b being temporarily left undefined and these constants later so chosen that the resistance law obtained agrees in two point, that is, at two Re_x numbers with the experiment, that is, the compensating curve IV in figure 6. So. rather than make an approximate assumption about the velocity distribution in direct wall proximity, a certain tangent is picked from out of the

$\frac{U}{v^*} = f\left(\frac{yv^*}{\nu}\right)$ or $\frac{U}{v^*} = f\left(\frac{y}{\delta}\right)$, respectively, the detailed

Equation (10) written in (8) gives the differential equation

$$\left(\frac{v^*}{U}\right) = \frac{d}{d\,Re_x}\left\{\frac{U}{v^*}\,e^{\frac{1}{b}\left(\frac{U}{v^*}-a\right)}\left[3.34\,\frac{v^*}{U} - 21.4\left(\frac{v^*}{U}\right)^2\right]\right\}$$

for $\frac{v^*}{U}$ and hence for c_f', since $\frac{v^*}{U} = \sqrt{2\,c_f'}$. Abbreviated it affords with

$$\frac{U}{v^*} = \eta; \quad Re_x = \zeta; \quad \frac{a}{b} = \beta$$

$$\frac{1}{\eta^2} = \frac{d}{d\zeta}\left\{e^{\frac{\eta}{b}-\beta}\left(3.34 - \frac{21.4}{\eta}\right)\right\}$$

whence by differentiation

$$\frac{1}{\eta^2} = \eta'\,e^{\frac{\eta}{b}-\beta}\left[\frac{1}{b}\left(3.34 - \frac{21.4}{\eta}\right) + \frac{21.4}{\eta^2}\right]$$

and by separation of variables

$$\zeta - \zeta_0 = \int_0^\eta e^{\frac{\eta}{b}-\beta}\left[\frac{1}{b}(3.34\,\eta^2 - 21.4\,\eta) + 21.4\right]d\eta$$

The integration affords

$$e^\beta(\zeta - \zeta_0) = e^{\frac{\eta}{b}}\left[3.34\,\eta^2 - (2\times3.34\,b + 21.4)\eta\right.$$
$$\left. + 2\times3.34\,b^2 + 21.4\,b + 21.4\right]_{\eta_0}^{\eta}$$

We integrate from $\zeta_0 = 0$. Then $\eta_0 = 0$ ($v^* = \infty$), whence the lower integration limit on the right-hand side is $2\times3.34b^2 + 21.4\,b + 21.4$. The value from the numerical evaluation ranged at around 100, while the upper integration limit lies at 10^7; in consequence of which the lower limit can be summarily disregarded. Then the solution reads:

$$\ln\zeta = \frac{\eta}{b} - \beta + \ln[3.34\,\eta^2 - (6.64\,b + 21.4)\eta$$
$$+ 6.64\,b^2 + 21.4(b + 1)] \quad (11)$$

which expresses our new resistance law, namely, the relationship between c_f' and Re. Now the constants b and β are so defined that (11) agrees with the experimental curve in two points.

This occurs when

$$b = 2.895; \quad \beta = 1.25$$

and so defines our tangent in the viscid fluid layer, with the exception of its position, since the velocity distribution in this immediate wall proximity is without effect on the momentum integral.

With the previously cited values of b and β it afforded agreement not only in the two points with the compensating curve IV of figure 6, but practically throughout the intermediate zone as well, thus furnishing an added proof of the universal validity of the obtained velocity distribution laws, and so permits an extrapolation of our resistance curve to any Reynolds number as exemplified in figure 9 as far as $Re_x = 2 \times 10^9$. The logarithmic law is also shown for comparison.

The total resistance coefficient c_f was numerically defined from figure 9 with the relation

$$c_f = \frac{1}{x} \int_0^x c_f' \, dx$$

readily derived from (2). It is reproduced in figure 10, along with the logarithmic law and the old power law. The departure of the logarithmic law is quite noticeable at the highest Re_x.

The approximate formulas for the two new resistance laws covering the range $10^6 \leq Re_x \leq 10^9$ are as follows:

$$c_f' = \frac{0.370}{(\log Re_x)^{2.584}}$$

$$c_f = \frac{0.427}{(-0.407 + \log Re_x)^{2.64}}$$

They correspond to the form of approximate formula proposed by Prandtl (reference 1)

$$c_f = \frac{m}{(\log \text{Re}_x + p)^n}$$

with which three points can be made to agree exactly and which was used also in the derivation of (4); p itself was found to be practically equal to zero in the derivation of the $c_f{}'$ formula, as in the derivation of (4).

SHEAR STRESS AND MIXING PATH DISTRIBUTION

The shear stress follows from the application of the momentum equation

$$\frac{\partial}{\partial x} \int_0^y u^2 \, dy + u \, v = \frac{\tau - \tau_0}{\rho}$$

TABLE I.- EVALUATION OF VELOCITY MEASUREMENT

[Average values: $\int_0^1 f_2 \, d\frac{y}{\delta} = 3.32, \int_0^1 (f_2)^2 \, d\frac{y}{\delta} = 21.4$]

x (m)	U (cm/s)	log (Re_x)	$\frac{y^*}{U}$	δ (cm)	δ* (cm)	ϑ (cm)	$\int_0^1 f_2 dy/\delta$	$\int_0^1 f_2{}^2 dy/\delta$	v_0 (cm/s)
0.5	1937	5.831	0.0444	1.30	0.187	0.131	3.20	21.9	-
1	1936	6.132	.0414	2.24	.306	.222	3.30	21.9	3.96
1.5	1942	6.308	.0398	3.07	.410	.301	3.36	22.3	3.67
2.5	1941	6.531	.0381	4.62	.584	.446	3.30	20.6	3.20
3.2	1941	.638	.0373	5.62	.700	.538	3.34	20.8	3.30
3.9	1938	6.723	.0367	6.60	.810	.624	3.35	21.0	3.45
5.3	1940	6.857	.0358	8.40	1.022	.796	3.40	21.0	-

Differentiation leaves

$$2 \int_0^y u \frac{\partial u}{\partial x}\, dy + u\,v = \frac{\tau - \tau_0}{\rho}$$

The continuity equation

$$v = - \int_0^y \frac{\partial u}{\partial x}\, dy$$

also exists. For the determination of $\frac{\partial u}{\partial x}$ the velocity distribution was plotted in figures 11 and 12 against different wall distances. The curve of $\frac{\partial u}{\partial x}$ is shown in figures 13, and 14, and that of the transverse velocity in figure 15; v_0 denotes the maximum transverse velocity which occurs at the edge of the friction layer. The separate v_0 values, compiled in the table disclose a maximum v_0 of about 2 percent of the flow velocity. Further evaluation gives the shear stress profiles of figure 16, concerning which it is stated that the equation of motion of a fluid particle past the plate (no pressure gradient) reads

$$u \frac{\partial u}{\partial x} + v \frac{\partial u}{\partial y} = - \frac{1}{\rho} \frac{\partial \tau}{\partial y}$$

But, at the wall, the fluid adheres whence $\frac{\partial \tau}{\partial y} = 0$ at that point. This condition for the initial tangent is not always satisfactory complied with on the reproduced shear stress profiles because of inaccuracies in the evaluation which are unavoidable on account of the differentiation of the $v(x)$ curve. At the most, the wall shear stresses obtained from this momentum interpretation are 5 percent greater than those obtained by balance measurement according to which the reliability of the evaluation can be gaged.

The mixing length is obtained from

$$\frac{\tau}{\rho} = l^2 \left(\frac{\partial u}{\partial y} \right)^2$$

and shown in figure 17. It now approaches at $\frac{y}{\delta} = 0.4$,

the constant mean value $\frac{1}{\delta}$ = 0.072. The relation for the wall tangent, l = 0.43y, does not vary appreciably from the relation l_R = 0.43y* ascertained on the pipe. A difference must exist by reason of the different shear stress profiles.

Translation by J. Vanier,
National Advisory Committee
for Aeronautics.

REFERENCES

1. Prandtl, L.: Zur turbulenten Strömung in Rohren und Längsplatten. Erg. Aerodyn. Vers.-Anst. zu Göttingen, IV Lieferg. (München), 1932, p. 18.

2. Gebers, F.: Ein Beitrag zur experimentellen Ermittlung des Wasserwiderstandes gegen bewegte Körper. Schiffbau, vol. 9, 1908.

3. Kempf, G.: Neue Ergebnisse der Widerstandsforschung. Werft, Reederei, Hafen, vol. 10, 1929, pp. 234 and 247.

4. Wieselsberger, C.: Untersuchungen über den Reibungswiderstand von stoffbespannten Flächen. Erg. Aerodyn. Vers.-Anst. zu Göttingen, I. Lieferg. (München), 1925, p. 120.

5. Prandtl, L.: Über den Reibungswiderstand strömender Luft. Erg. Aerodyn. Vers.-Anst. zu Göttingen, III. Lieferg. (München), 1927, p. 1.

6. Schönherr, K.: Resistance of Flat Plates. Trans. Soc. Naval Architects and Marine Engrs., vol. 40, 1932.

7. Prandtl, L.: Recent Results of Turbulence Research. T.M. No. 720, NACA, 1933.

---

*The average value of large and small Reynolds numbers is 0.4. At high Reynolds numbers the value is 0.415.
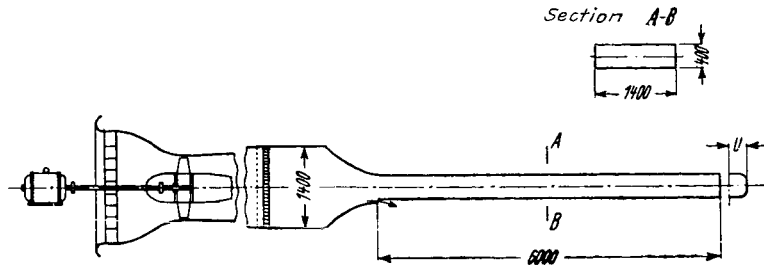
Figure 1.- Experimental setup.
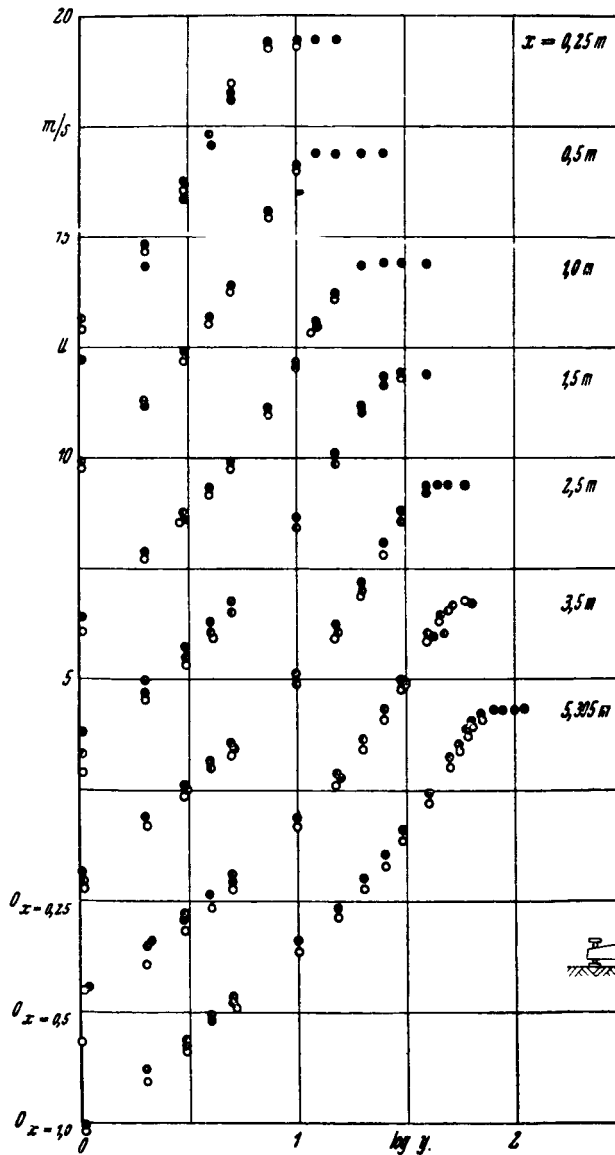
Figure 2.- Velocity profiles on the experimental wall; Y in mm.
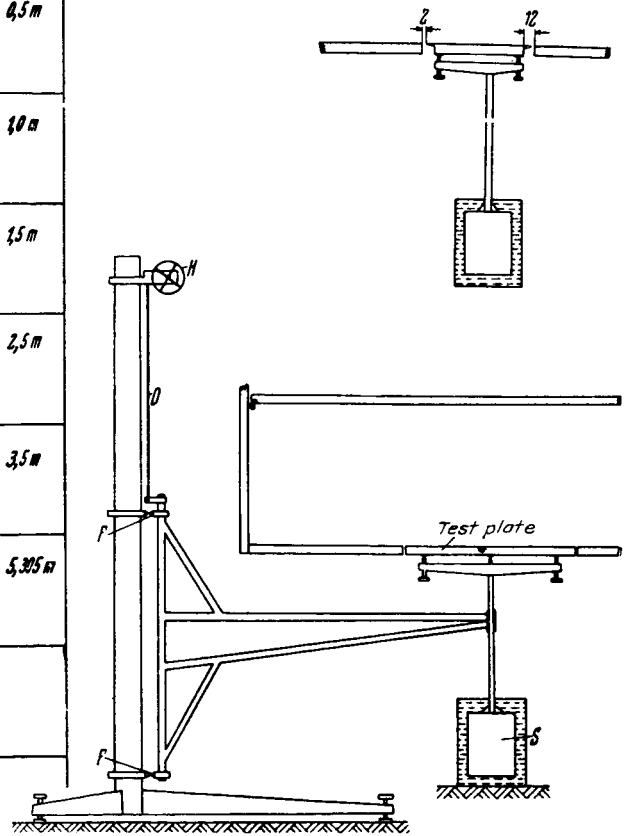
Figure 3.- Arrangement of test plate and balance.

H, hand wheel
D, wire
F, spring hinge
S, float
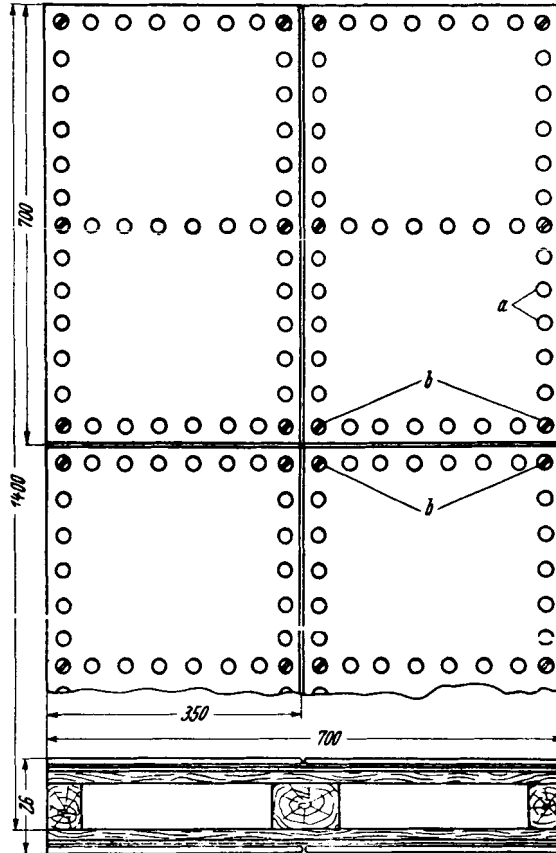
Figure 4.- Surface C; flush riveted; arrangement of rivets and screws,
a, flush rivets
b, countersunk wood screws, not covered.
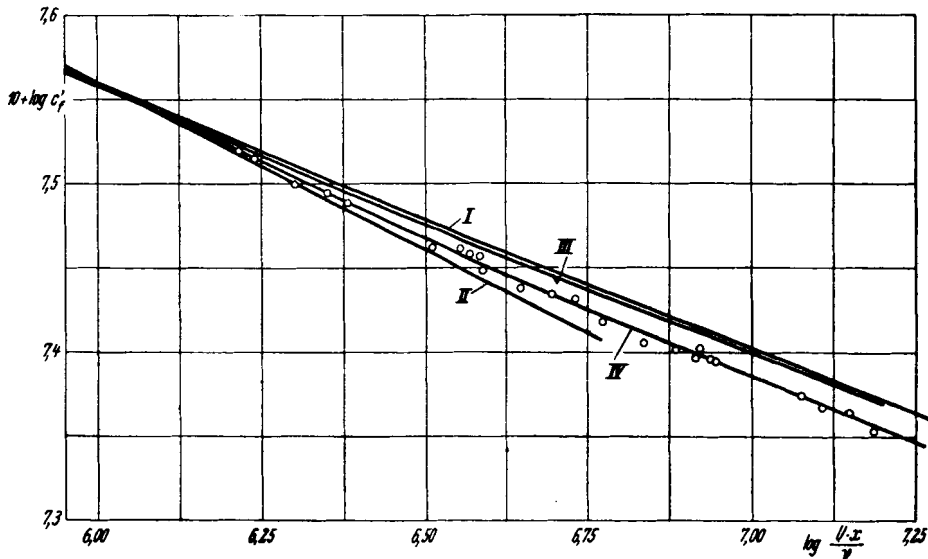
Figure 5.- Momentum displacement and friction layer
thickness δ, δ^*, ϑ on surface A (built-up
laminated plate), U = 19.4m/s.
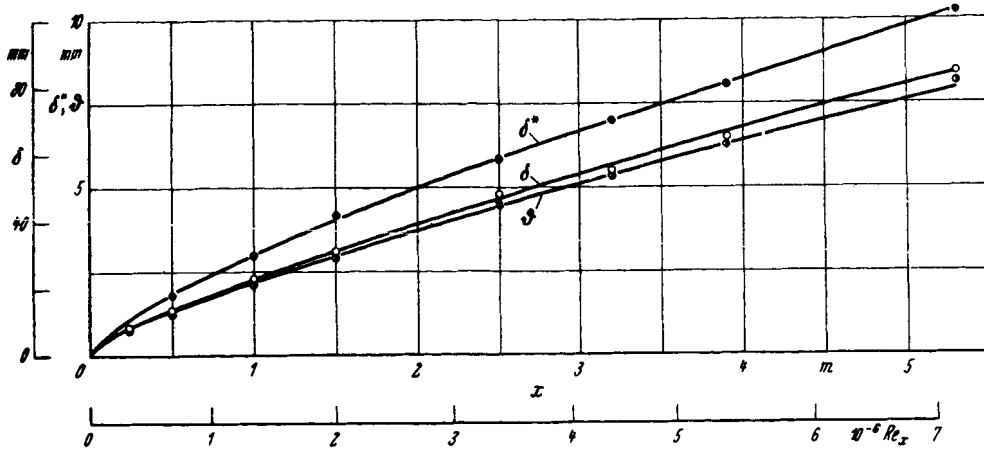
Figure 6.- Local drag coefficient of surface A,
    I, calculated from Kempf's pipe test (logarithmic
        resistance law),
   II, old power formula $c_f = 0.0576 \, Re_x^{-1/5}$
  III, Schoenherr's empirical formula,
   IV, compensating curve through test points.
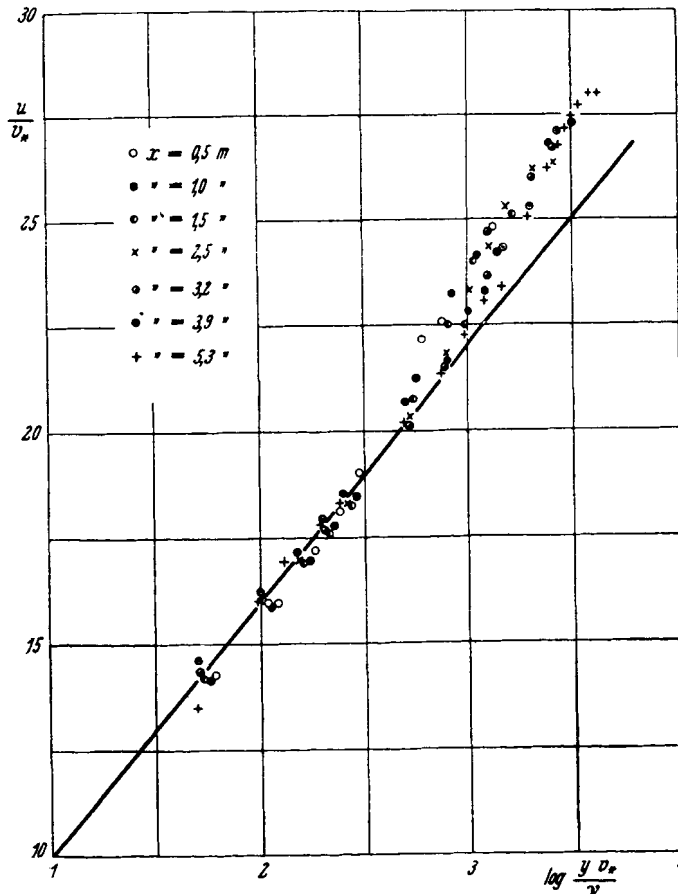
Figure 7.-

Velocity
profiles
on plate.
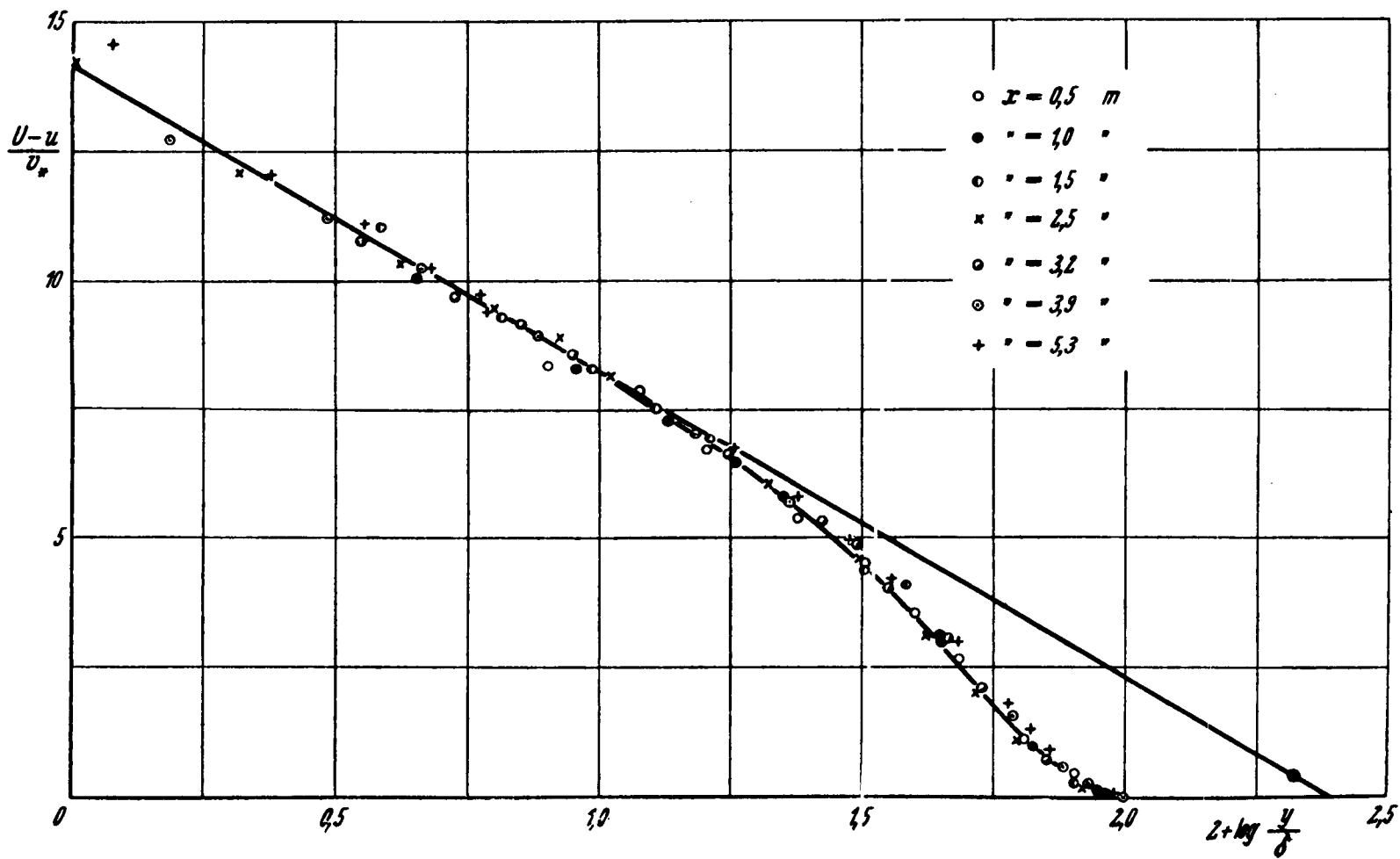
Figure 8.- Velocity profiles on plate.

Fig. 8

I. New resistance law.
II. Logarithmic resistance law.
III. Old power formula, $c_f = 0.072 \, Re_x \, -1/5$.
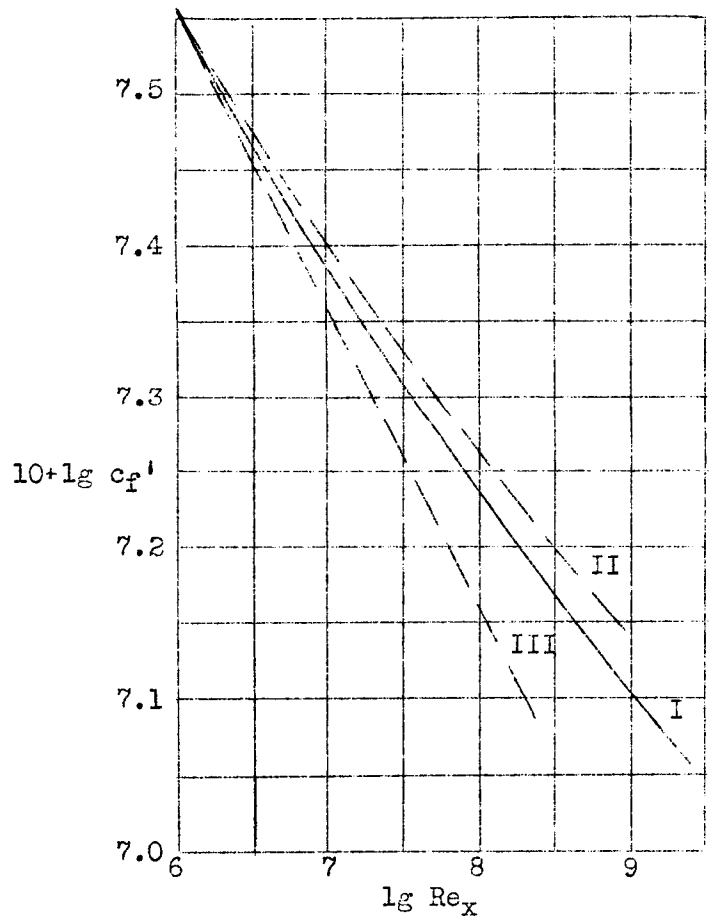
Figure 9.- New resistance law for smooth
plate, c_f' curve.
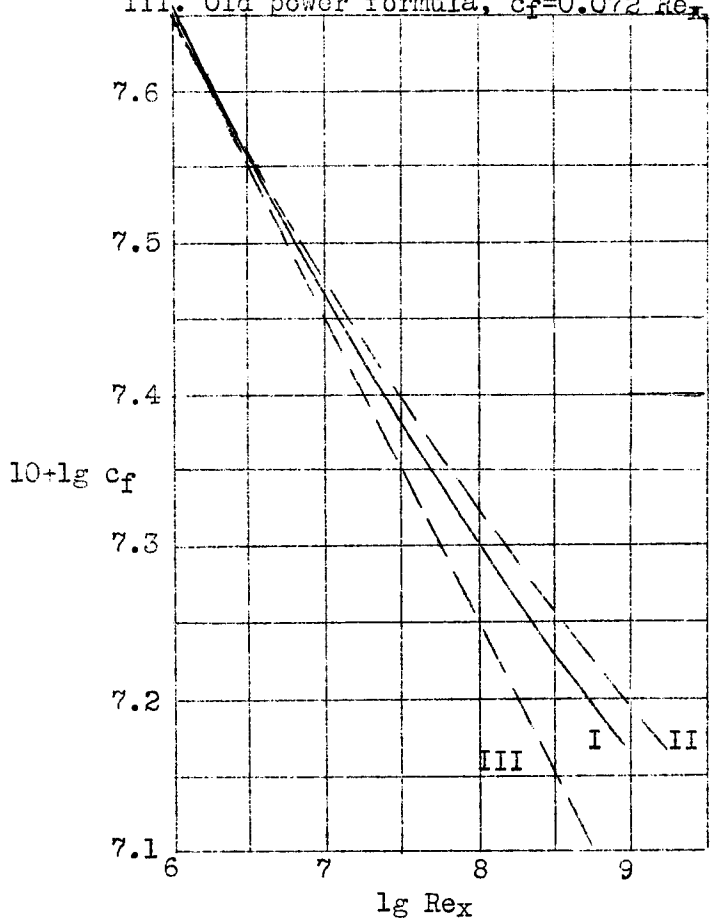
Figure 10.- New resistance law for smooth
plate, c_f curve.

Figure 11.- Velocity distribution
at different wall dis-
tances, U = 19.4 m/s.
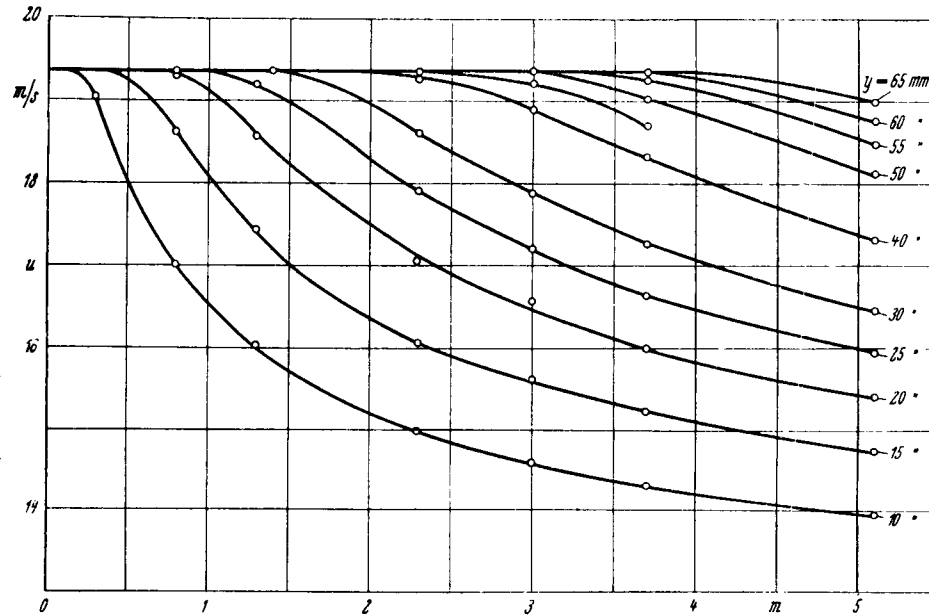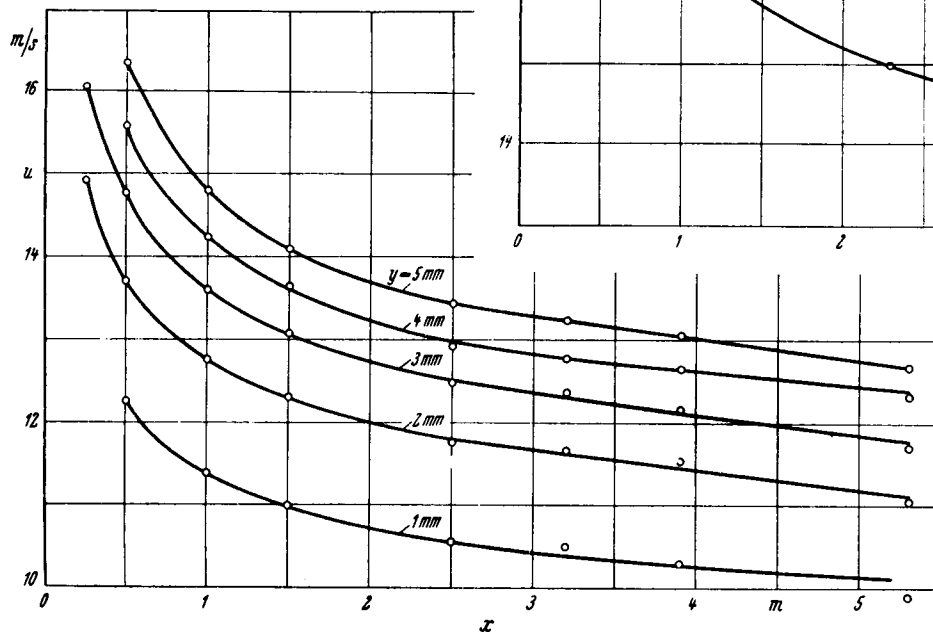
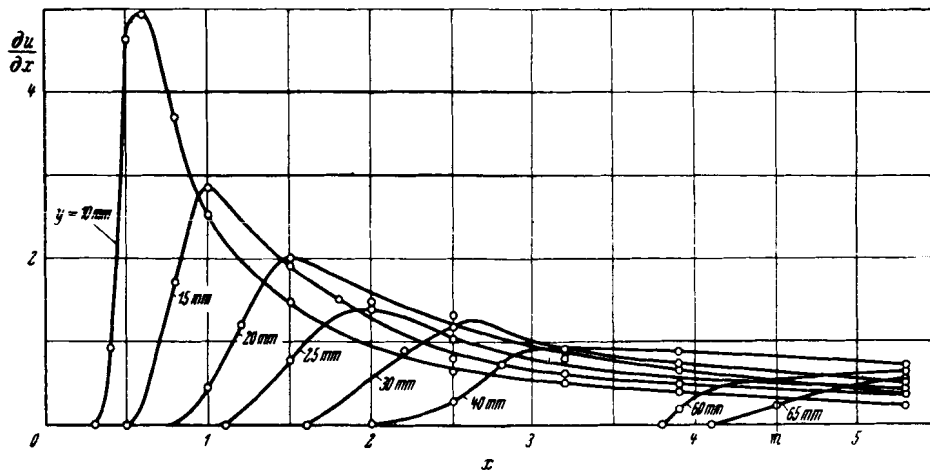Figure 12.-

Velocity distribution
at different wall dis-
tances, U = 19.4 m/s.

Figures 13, 14.-
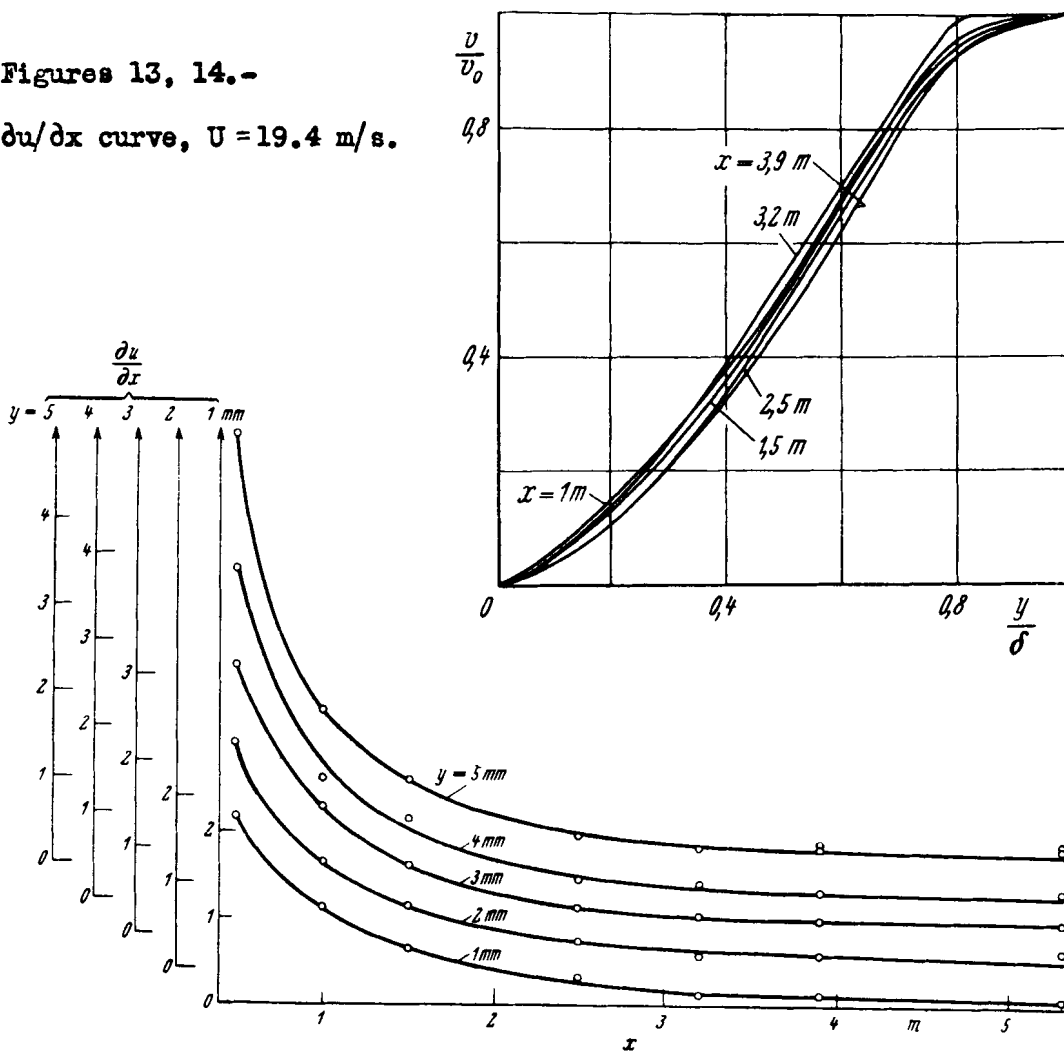
$\partial u / \partial x$ curve, U = 19.4 m/s.

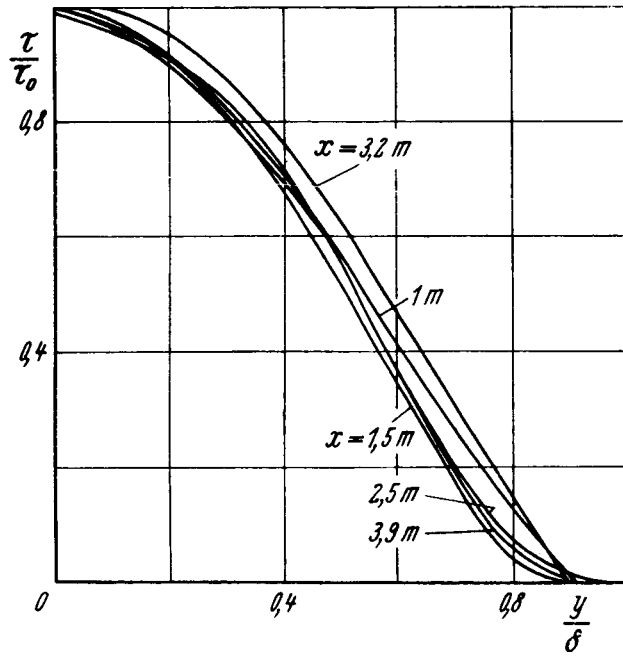
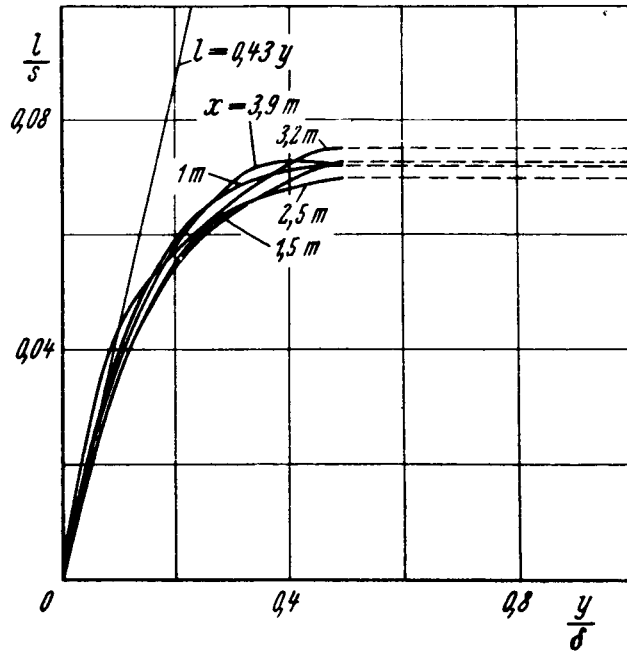Figure 15.- Transverse velocity **v**,
U = 19.4 m/s.

Figure 16.- Shear-stress profiles,
U = 19.4 m/s.

Figure 17.- Curve of mixing path.